NASA/CR—2008-215199

Microstructure Modeling of 3rd Generation Disk Alloy

Herng-Jeng Jou
QuesTek Innovations LLC, Evanston, Illinois

April 2008

NASA STI Program . . . in Profile

Since its founding, NASA has been dedicated to the advancement of aeronautics and space science. The NASA Scientific and Technical Information (STI) program plays a key part in helping NASA maintain this important role.

The NASA STI Program operates under the auspices of the Agency Chief Information Officer. It collects, organizes, provides for archiving, and disseminates NASA's STI. The NASA STI program provides access to the NASA Aeronautics and Space Database and its public interface, the NASA Technical Reports Server, thus providing one of the largest collections of aeronautical and space science STI in the world. Results are published in both non-NASA channels and by NASA in the NASA STI Report Series, which includes the following report types:

- TECHNICAL PUBLICATION. Reports of completed research or a major significant phase of research that present the results of NASA programs and include extensive data or theoretical analysis. Includes compilations of significant scientific and technical data and information deemed to be of continuing reference value. NASA counterpart of peer-reviewed formal professional papers but has less stringent limitations on manuscript length and extent of graphic presentations.

- TECHNICAL MEMORANDUM. Scientific and technical findings that are preliminary or of specialized interest, e.g., quick release reports, working papers, and bibliographies that contain minimal annotation. Does not contain extensive analysis.

- CONTRACTOR REPORT. Scientific and technical findings by NASA-sponsored contractors and grantees.

- CONFERENCE PUBLICATION. Collected papers from scientific and technical conferences, symposia, seminars, or other meetings sponsored or cosponsored by NASA.

- SPECIAL PUBLICATION. Scientific, technical, or historical information from NASA programs, projects, and missions, often concerned with subjects having substantial public interest.

- TECHNICAL TRANSLATION. English-language translations of foreign scientific and technical material pertinent to NASA's mission.

Specialized services also include creating custom thesauri, building customized databases, organizing and publishing research results.

For more information about the NASA STI program, see the following:

- Access the NASA STI program home page at *http://www.sti.nasa.gov*

- E-mail your question via the Internet to *help@sti.nasa.gov*

- Fax your question to the NASA STI Help Desk at 301–621–0134

- Telephone the NASA STI Help Desk at 301–621–0390

- Write to:
  NASA Center for AeroSpace Information (CASI)
  7115 Standard Drive
  Hanover, MD 21076–1320

NASA/CR—2008-215199

Microstructure Modeling of 3rd Generation Disk Alloy

Herng-Jeng Jou
QuesTek Innovations LLC, Evanston, Illinois

Prepared under Contract NNC07CB01C

National Aeronautics and
Space Administration

Glenn Research Center
Cleveland, Ohio 44135

April 2008

This report contains preliminary findings, subject to revision as analysis proceeds.

Level of Review: This material has been technically reviewed by NASA technical management.

Available from

NASA Center for Aerospace Information
7115 Standard Drive
Hanover, MD 21076–1320

National Technical Information Service
5285 Port Royal Road
Springfield, VA 22161

Available electronically at http://gltrs.grc.nasa.gov

Executive Summary

The objective of this initiative, funded by NASA's Aviation Safety Program, is to model, validate, and predict, with high fidelity, the microstructural evolution of third-generation high-refractory Ni-based disc superalloys during heat treating and service conditions. This initiative is a natural extension of the DARPA-AIM (Accelerated Insertion of Materials) initiative with GE/Pratt-Whitney and with other process simulation tools. Strong collaboration with the NASA Glenn Research Center (GRC) is a key component of this initiative and the focus of this program is on industrially relevant disk alloys and heat treatment processes identified by GRC. Employing QuesTek's Computational Materials Dynamics technology and PrecipiCalc precipitation simulator, physics-based models are being used to achieve high predictive accuracy and precision. Combining these models with experimental data and probabilistic analysis, "virtual alloy design" can be performed. The predicted microstructures can be optimized to promote desirable features and concurrently eliminate nondesirable phases that can limit the reliability and durability of the alloys. The well-calibrated and well-integrated software tools that are being applied under the proposed program will help gas turbine disk alloy manufacturers, processing facilities, and NASA, to efficiently and effectively improve the performance of current and future disk materials.

Contents

Introduction

In support of higher fidelity application of the DARPA-AIM acceleration methodology previously demonstrated on the IN100 and R88DT disc alloys, a collaborative model and database validation study is supported by the NASA Aviation Safety Program to better quantify uncertainty and improve prediction accuracy of the QuesTek PrecipiCalc (ref. 5) multiphase/multicomponent precipitation simulation code. The nominal compositions of relevant disk alloys are tabulated in Table 1.

TABLE 1.—NOMINAL COMPOSITIONS (WT%) OF THE DISK ALLOYS STUDIED UNDER THIS PROGRAM

at.%	Ni	Cr	Co	Mo	W	Al	Ti	Nb	Ta	C	B	Zr
ME3	Bal.	13.1	20	3.8	1.9	3.5	3.6	1.1	2.3	0.04	0.03	0.05
LSHR	Bal.	13	21	2.7	4.3	3.5	3.5	1.5	1.6	0.03	0.03	0.05
Alloy10	Bal.	10.2	14.9	2.7	6.2	3.7	3.9	1.9	0.9	0.03	0.03	0.1
RR1000	Bal.	15	18.5	5	---	3	3.6	---	2	0.027	0.015	0.06

Program Status

The program is on schedule for this reporting period. Major accomplishments for this reporting period are detailed in the Gantt chart in Figure 1.

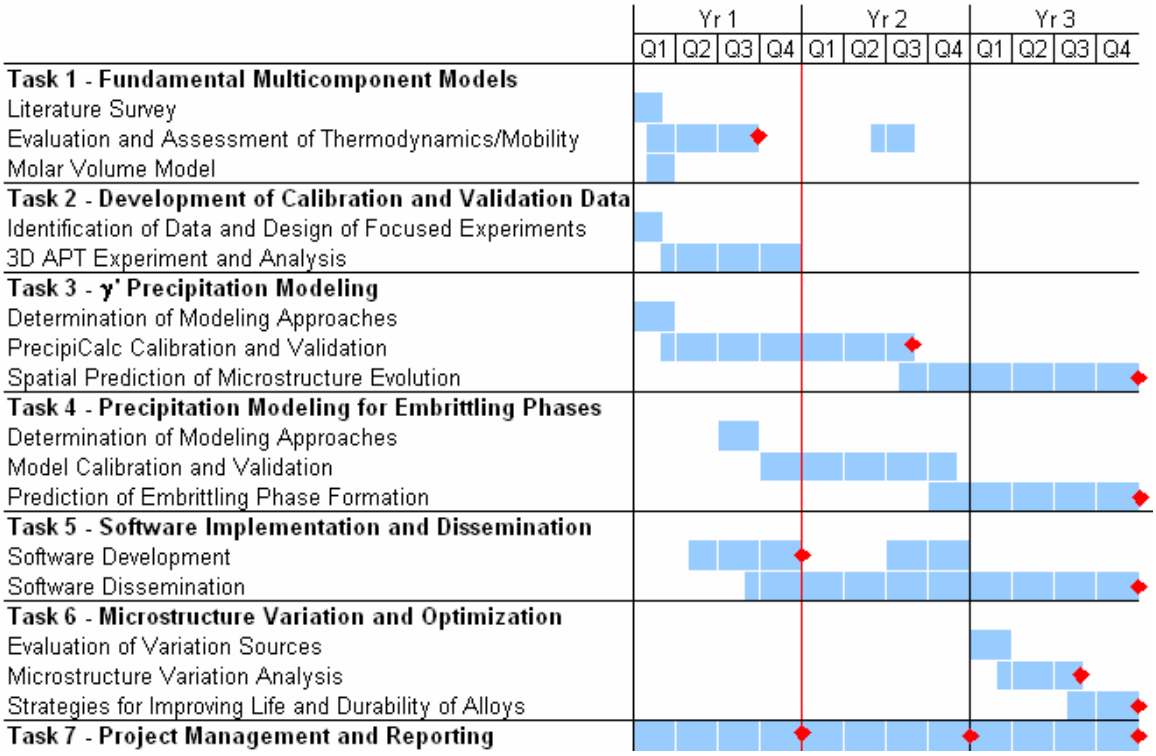

Figure 1.—Project Gantt chart of the proposed work.

Task 1—Fundamental Multicomponent Models

Thermodynamics

Our assessment indicates that Ni-DATA version 7 in combination with NIST-Mobility is most favorable, because it reproduces the γ'-phase precipitation behavior accurately in Ni-Al-Cr and Ni-Al-Cr-X (X = Re, W) model alloys, as well as in commercial disc alloys. Thermodynamic databases compared in this study include ThermoTech Ni-DATA versions 4 to 7 (ref. 12), Ni-NIST (not including Nb) (ref. 1), Thermo-Calc TCNI1 (not including Mo, Nb, and Ta) (ref. 3), and CompuTherm PanNickel (ref. 11) in combination with NIST-Mobility (ref. 2) and MOBNi1 (ref. 10). Compared to previous versions, Ni-DATA version 7 contains updates to improve the γ'-phase solvus temperature prediction for recently developed Ni-base alloys with high refractory elements. The equilibrium concentrations calculated with Ni-DATA version 7 are in good agreement with the equilibrium concentrations at infinite time. See Table 2 for the comparison summary for the Ni-Al-Cr system, where Ni7 was found to be best, according to the root mean square (RMS) analysis.

TABLE 2.—COMPARISON AND ANALYSIS OF COMPOSITIONS FROM APT MEASUREMENT AND THERMODYNAMICS EQUILIBRIUM PREDICTIONS WITH VARIOUS DATABASES FOR A Ni-Al-Cr SYSTEM

			at.%					600 °C	
	600 °C		Ni	Al	Cr	APB	RMS	misfit	γ' vol. frac.
γ	Equilibrium matrix	APT	81.26	3.13	15.61				
		2σ	0.18	0.08	0.18		0.14		
		Ni5	81.40	3.64	14.96		0.82		
		Ni6	81.40	3.64	14.96		0.82		
		Ni7	**81.34**	**3.62**	**15.04**		**0.75**		
		TCNI1	81.17	3.93	14.90		1.07		
		Ni-NIST	80.60	5.20	14.20		2.50		
γ'	Equilibrium composition of γ'-precipitates	APT	76.53	16.69	6.77	0.19		–0.72%	14.8%
		2σ	0.50	0.44	0.30	0.01	0.38		0.5%
		Ni5	74.98	16.23	8.80	0.19	2.08	–0.58%	12.4%
		Ni6	74.98	16.23	8.80	0.19	2.08	–0.58%	12.4%
		Ni7	**74.97**	**16.21**	**8.82**	**0.19**	**2.11**	**–0.57%**	**12.4%**
		TCNI1	75.59	14.55	9.57	0.18	3.52	–0.75%	12.3%
		Ni-NIST	75.96	12.25	11.79	0.15	6.70	–0.89%	0.0%
	Critical γ'-nucleus composition	APT	72.40	18.30	9.30	0.16		–0.22%	
		2σ	2.20	1.80	1.40	0.03	1.61		
		Ni5	74.91	17.37	7.71	0.20	1.84	–0.52%	
		Ni6	74.91	17.37	7.71	0.20	1.84	–0.52%	
		Ni7	**74.91**	**17.40**	**7.69**	**0.20**	**1.84**	**–0.51%**	
		TCNI1	75.36	16.43	8.21	0.19	2.16	–0.61%	
		Ni-NIST	No precipitation						

The comparisons in Ni-10Al-8.5Cr-2X (X = Re, W) model alloys again support Ni-Data version 7 as most accurate. In the Ni-Al-Cr-Re alloy, the phase relations measured by Yoon et al. (ref. 8) suggest a partial solute-trapping behavior of slow-diffusing species Re, see Table 3.

TABLE 3.—COMPARISON AND ANALYSIS OF COMPOSITIONS FROM APT MEASUREMENT AND THERMODYNAMICS EQUILIBRIUM PREDICTIONS WITH VARIOUS DATABASES FOR A Ni-Al-Cr-RE SYSTEM

	800 °C		Ni	Cr	Al	Re	APB	RMS	misfit	γ' vol. frac.
γ	Equilibrium matrix	APT	81.07	10.04	6.74	2.15				
		2σ	0.16	0.04	0.08	0.02		0.09		
		Ni7	**80.55**	**8.94**	**8.35**	**2.16**		**1.95**		
		Ni-NIST	80.22	8.79	8.87	2.12		2.47		
γ'	Equilibrium composition of γ'-precipitates	APT	76.17	4.97	18.05	0.81	0.19		–0.71%	25.4%
		2σ	0.26	0.10	0.18	0.04	0.00	0.21		0.2%
		Ni7	**75.29**	**5.68**	**18.80**	**0.23**	**0.20**	**1.18**	**–0.68%**	**15.9%**
		Ni-NIST	75.82	6.13	17.65	0.39		1.30	–0.77%	7.2%
	80% equilibrium composition of γ'-precipitates	APT	76.33	5.46	16.92	1.29	0.17			20.3%
		2σ	0.30	0.16	0.26	0.08	0.00	0.32		0.3%
		Ni7	**75.22**	**5.56**	**18.99**	**0.23**	**0.20**	**2.33**		**12.8%**

TABLE 4.—COMPARISON AND ANALYSIS OF COMPOSITIONS FROM APT MEASUREMENT AND THERMODYNAMICS EQUILIBRIUM PREDICTIONS WITH VARIOUS DATABASES FOR ANi-Al-Cr-W SYSTEM

	800 °C		Ni	Al	Cr	W	APB	RMS	misfit	γ' vol. frac.
γ	Equilibrium matrix	APT	81.31	5.83	11.52	1.34				
		2σ	0.07	0.04	0.05	0.02		0.07		
		Ni7	**81.44**	**6.22**	**10.53**	**1.80**		**1.16**		
		Ni-NIST	80.48	8.57	8.84	2.11		3.91		
γ'	Equilibrium composition of γ'-precipitates	APT	76.30	17.00	3.91	2.80	0.21		–0.49%	38.2%
		2σ	0.08	0.07	0.04	0.03	0.00	0.09		0.1%
		Ni7	**75.39**	**18.00**	**4.20**	**2.42**	**0.22**	**1.11**	**–0.36%**	**32.1%**
		Ni-NIST	75.87	16.61	6.42	1.09		3.06	–0.61%	18.7%

Composition trajectories of isothermal γ' precipitation in simple Ni-Al-Cr-X alloys were examined. In a Ni–5.2Al–14.2Cr at.% alloy during isothermal precipitation at 1112 °F (600 °C), Sudbrack et al. (ref. 7) at the Northwestern University Center for Atom Probe Tomography (NUCAPT) reported the γ/γ' interfacial free energy as 22 to 23 mJ/m^2. They also reported that the effective solute diffusivities are one order of magnitude smaller than the predicted intrinsic diffusivities in the matrix phase. Employing these values, the simulation results for the evolution of phase fraction and particle size are consistent with their Atom-Probe Tomography (APT) analysis.

The time evolution of particle size measured by APT suggests the precipitation composition trajectory can be modeled as an unstable equilibrium with capillarity. The composition trajectory calculated by PrecipiCalc in the parallel tangent composition mass balance mode is consistent with the unstable equilibrium Thermo-Calc (ref. 13) calculations by adding capillary energy. However, our simulation results underestimate the Cr-enrichment in the γ' critical nucleus. As Cr reduces the interphase lattice misfit, an elastic energy could be added to the γ' free energy in our thermodynamic calculations to account for this.

To further examine the solute-trapping behavior of slow-diffusing refractory elements such as Mo, Hf, Ta, W, and Re, we conducted a literature review on the diffusivity of these species. Karunaratne and Reed (ref. 4) reported interdiffusion coefficients estimated by diffusion profile measurements. In dilute additions, the interdiffusion coefficients display little concentration dependence, but the values can differ by an order of magnitude. A systematic trend is observed: elements furthest from the center of the

periodic table display the largest values and elements at the center the smallest. W and Re are most potent for retarding the γ' coarsening kinetics, and in turn most prone to kinetic trapping.

However, Sudbrack et al. (ref. 6) report no such solute-trapping in Ni-10Al-8.5Cr-2W aged at 1472 °F (800 °C) up to 264 hr. The prolonged aging seems to eliminate the trapping behavior. Also, we confirmed that prolonged aging eliminates trapping for W in ME3. Thus, there is no apparent need to account for solute-trapping in our thermodynamic calculations.

The equilibrium concentrations in Ni-10Al-8.5Cr-2W calculated with Ni-DATA version 7 are in good agreement with the extrapolated equilibrium concentrations. Comparisons of γ' phase fraction and the at-temperature interphase lattice-parameter misfit with the database predictions for these alloys again support the Ni-DATA version 7 database as most accurate, and suggest the corresponding error in APB energy and misfit is acceptable within current structure/property model uncertainty.

Mobility

To assess accuracy of available atomic mobility databases for combination with thermodynamic databases to predict multicomponent diffusivities, linear diffusion multiples were prepared by Dr. Ivan Locci at the NASA Glenn Research Center. A 0.2-in. thick disk of pure Ni was diffusion bonded by hot pressing to a 0.125-in. thick disk of ME3 on one side and to a 0.125-in. thick of Alloy 10 on the other, for 4 hr at 1610 °F in vacuum. After the initial bond was formed, the diffusion couple was subjected to additional annealing in a horizontal tube furnace in an argon atmosphere at two temperatures, 2000 °F (1093 °C) or 1700 °F (927 °C) for 100 or 300 hr.

QuesTek's DICTRA (ref. 9) simulations with Ni-DATA version 7 and NIST-Mobility of the diffusion multiple at the hot-pressing temperature 1400 °F predict no significant diffusion, as shown below in figure 2. Therefore, subsequent simulations are ignoring the hot-pressing step.

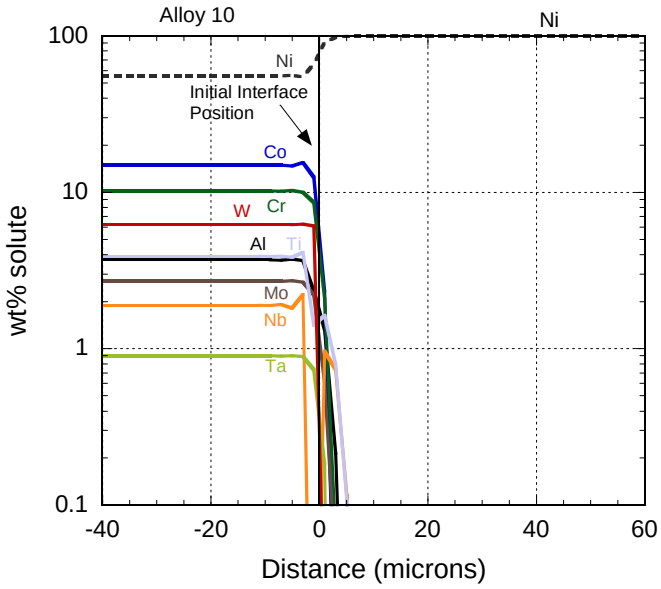

Figure 2.—DICTRA predicted composition trajectories of the Alloy10-Ni diffusion couple after 1400 °F hot press.

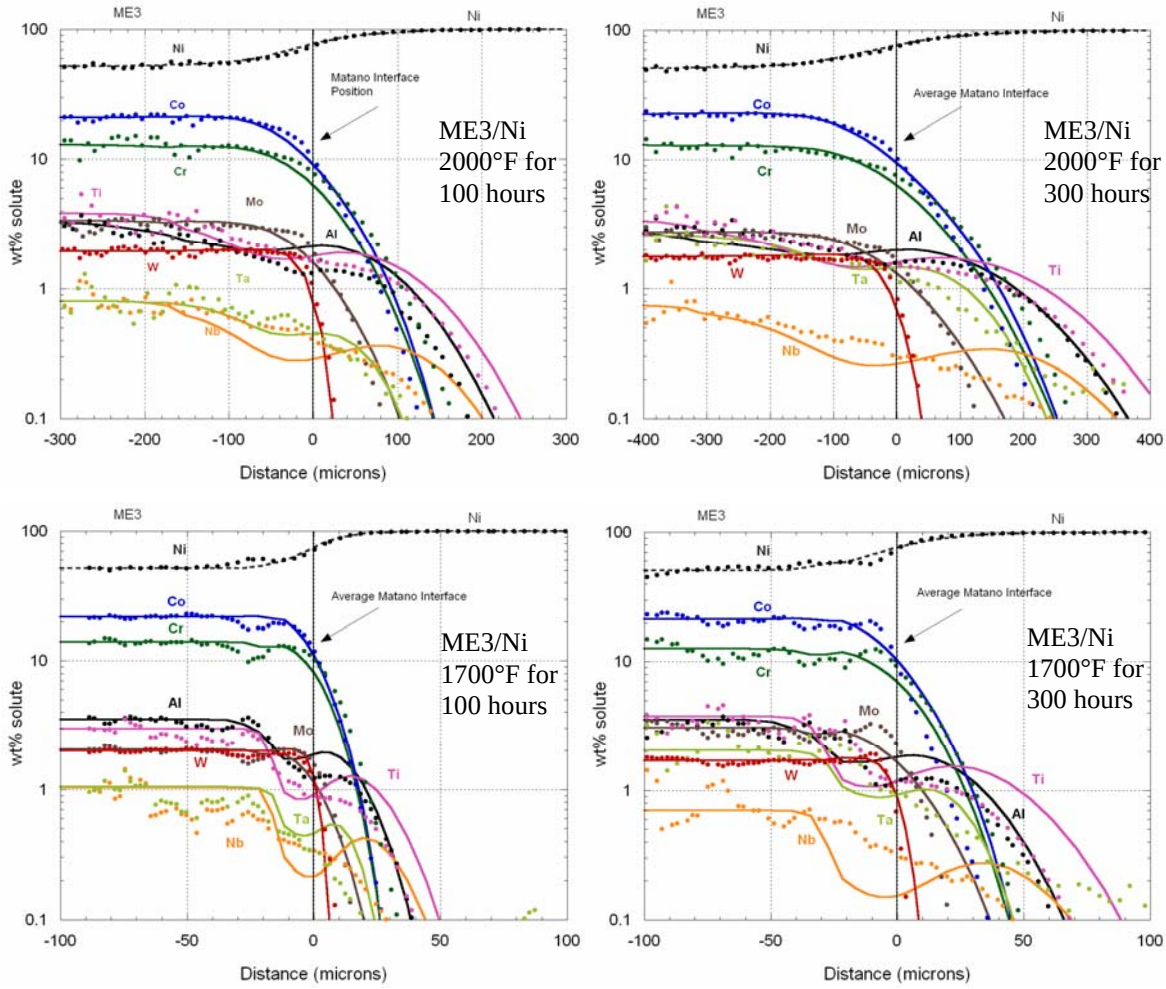

Figure 3.—Comparison of microanalysis and DICTRA predicted composition traces of the ME3-Ni diffusion couples at different aging conditions.

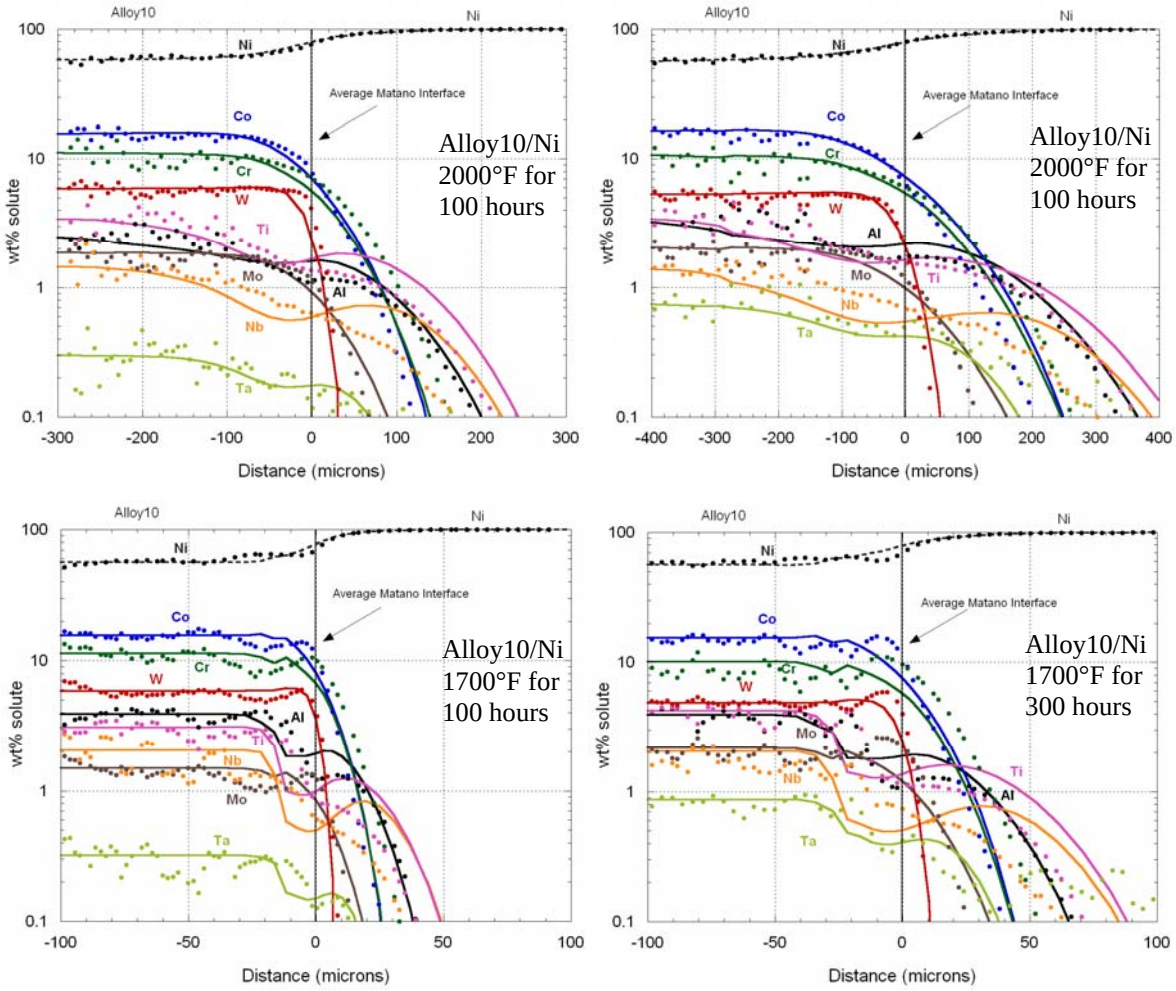

Figure 4.—Comparison of microanalysis and DICTRA predicted composition traces of the Alloy10-Ni diffusion couples at different aging conditions.

The NIST mobility database employed in the AIM project was compared with the Thermo-Calc MOB1 database in combination with various thermodynamic databases for ME3, Figure 3, and Alloy 10, Figure 4. In order to compare microprobe analyses of the diffusion multiple with DICTRA simulations, the average Matano interface (defined as the interface across which equal number of atoms have crossed in both directions) was equated to the origin of the calculated profiles. Assuming γ' precipitates act only as sink or source of solute for diffusion, i.e. no diffusion through γ', the agreement is reasonable for Co, Cr, Mo, and W in ME3/Ni diffusion couple held at 2000 °F (1093 °C) for 100 hr. Before setting the Matano interface as the origin, a significant discrepancy was noticed for W; however this was resolved with the Matano interface adjustment. With the exception of Al, the data does not confirm the predicted strong nonmonotonic profiles near the interface.

Furthermore, the current comparison shows that the diffusion of Nb, Ta, Al, and Ti is less than predicted. Of these elements, Ta seems to suffer from microprobe detection efficiency. Nb, Al, and Ti are γ'-stabilizers and could be affected by the no-diffusion-through-γ' assumption. Dr. Misra from QuesTek Innovations will present these results at the upcoming NIST diffusion workshop. The results were then forwarded to Dr. Campbell at NIST for a mobility database calibration. If needed, the diffusion multiple will be heat-treated at a supersolvus temperature to eliminate complications from precipitates. Nonetheless, the predicted transition width between γ+γ'+MC and γ is in excellent agreement with experimental measurement.

Molar Volume

Comparison of relative interphase misfit provides a useful metric of database accuracy for the complex disc alloys. The molar volume model constructed in QuesTek's prior AIM program was applied to calculate the lattice misfit in disk alloys. A model was implemented at QuesTek to calculate the nonmonotonic temperature dependency of lattice misfit, see Figure 5. The disc alloys fall into 2 groups of relatively high and low misfit. ME3, LSHR, and Alloy 10 show large positive misfit, consistent with the aligned precipitates observed in SEM. Of the third-generation disc alloys, only the RR1000 alloy is predicted to maintain the low misfit of the IN100 and R88DT alloys. In support of this prediction, while the fine intragranular precipitates in Alloy10 show the cuboidal morphology and ordered arrays consistent with the predicted higher misfit, the γ' in RR1000 shows a spheroidal morphology and disordered distribution consistent with its predicted low misfit, see Figure 6.

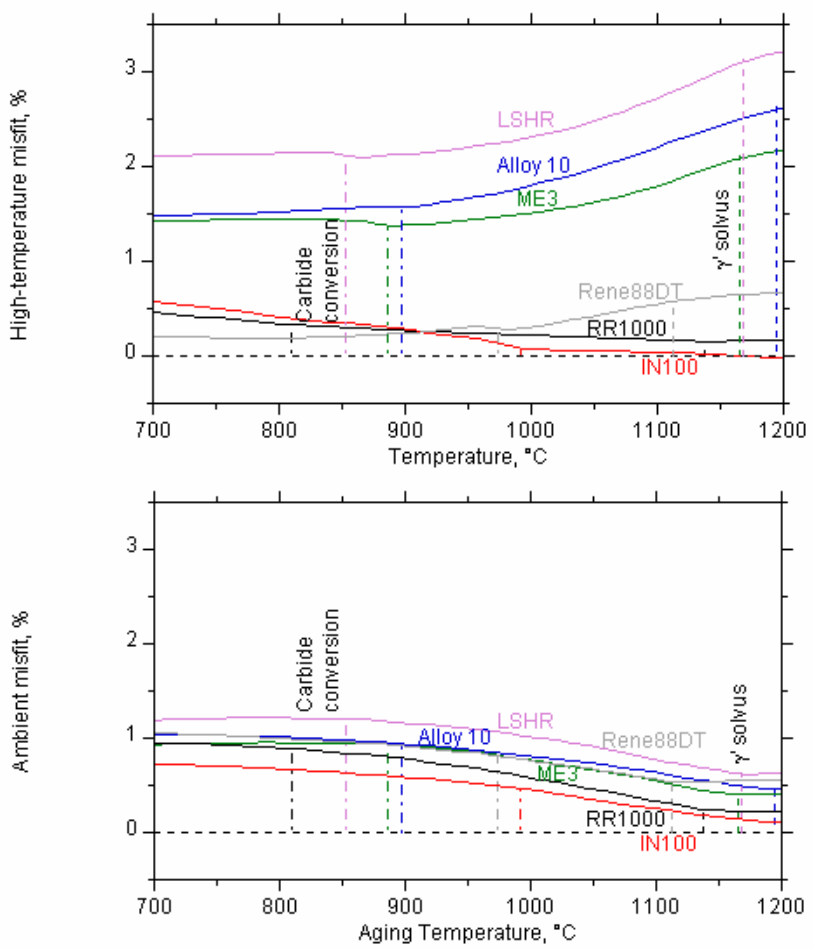

Figure 5.—Predicted γ'/γ misfit at high and ambient temperatures based on γ'/γ compositions calculated by equilibrium.

Alloy10 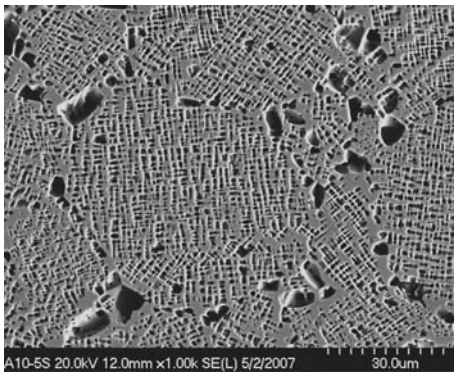

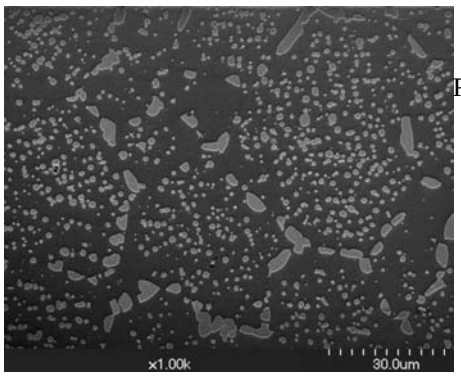

RR1000

Figure 6.—Experimentally observed γ' microstructure of Alloy10 and RR1000.

Task 2—Development of Calibration and Validation Data

High Temperature Equilibrium Age Results

To assess equilibrium phase fractions and compositions in commercial disc alloys, samples of ME3, LSHR, Alloy10 and RR1000 disc alloys were given a supersolvus treatment at 2190 °F (1199 °C) followed by water quench, and subsequent 20~1000-hr treatments at temperatures of 2000 °F (1093 °C), 1700 °F (930 °C), and 1400 °F (760 °C). Local Electrode Atom Probe (LEAP) at Northwestern University was used to analyze the composition and fine γ' microstructure of selected samples. Like a traditional 3-Dimensional Atom Probe (3DAP), the LEAP microscope by Imago Scientific Instruments achieves true 3-dimensional atomic-scale analysis by using a high electric field to remove individual atoms from material surfaces and a position-sensitive detector to record information that reveals the atom's position and identity. The incorporation of a local electrode eliminates or mitigates many of the performance limitations of traditional 3DAPs. The LEAP microscope at Northwestern University analyzes significantly larger volumes in much less time, compared to the traditional 3DAP.

The first sample analyzed under LEAP was ME3 water quenched from 2190 °F (1199 °C). In total, 8.7 million atoms were analyzed with the new larger-FOV LEAP detector. The overall bulk composition is very close to the expected composition. The precipitates formed during quenching have a sphere-equivalent diameter of about 15 to 30 nm. They are enriched predominantly in Ni-Ti-Al-Ta, and also in Nb, B, C, and O. They are depleted predominantly in Cr-Co-Mo, and also somewhat in W, Fe, and Si. The measured compositions show good agreement with our multiphase *PrecipiCalc* simulation.

In addition, the high-temperature matrix composition of ME3 aged at 2000 °F for 1000 hr was also analyzed by LEAP. 6.2 million atoms were analyzed with the new larger-FOV LEAP detector. The precipitates formed during quenching are enriched predominantly in Ni-Ti-Al-Ta, and also in Nb, B, C, and O. They are depleted predominantly in Cr-Co-Mo, see Figure 7, similar to the results from ME3 water quench sample. Also, the slow-diffusing W showed solute-trapping behavior in γ' nanoscale particles. The measured compositions are compared with our multiphase *PrecipiCalc* simulation, see Table 5.

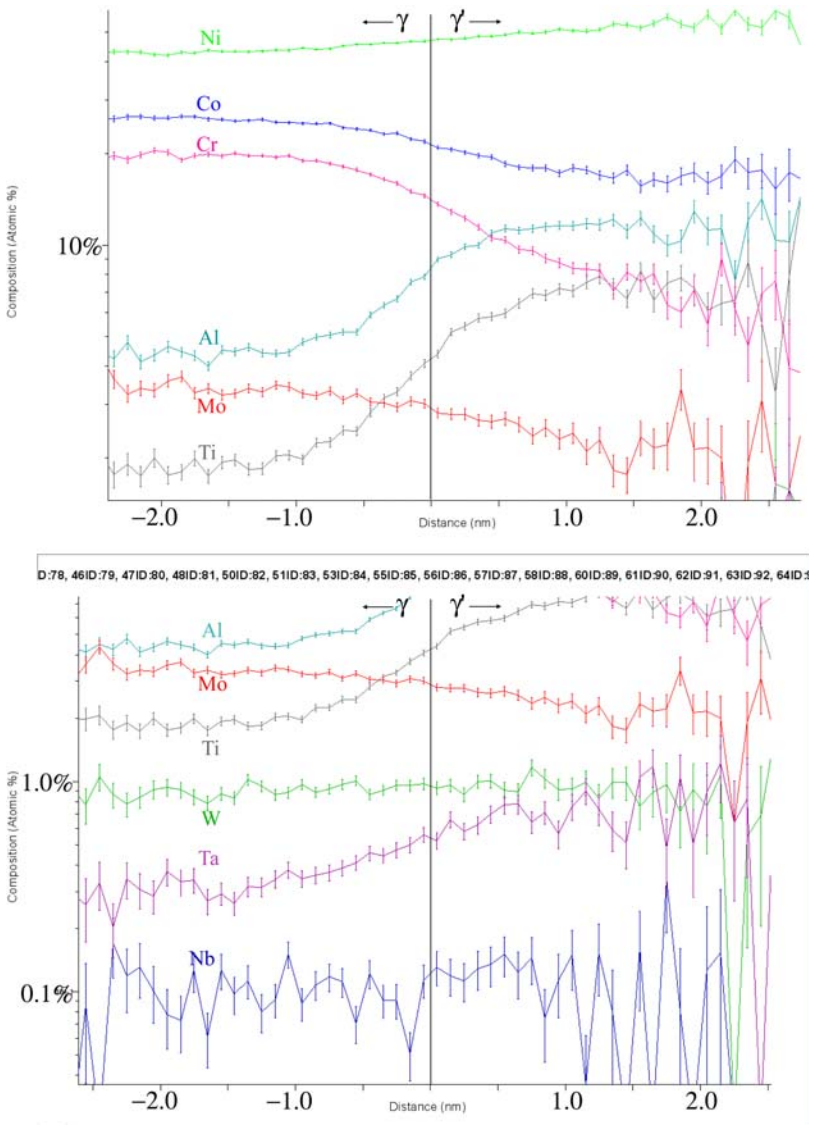

Figure 7.—γ and γ' composition analysis of LEAP experiment on ME3 2000 °F/1000 hr isothermal hold sample. Only fine γ' particles (formed during quench from 2000 °F) were observed in LEAP.

An experimental γ' and MC phase fraction at 2000 °F equilibrium were determined to be 24.8±1.5 and 0.33 percent, respectively, by mass-balancing the LEAP measurement and calculated γ' and MC phase compositions. At bottom of Table 5, it is clearly seen that Ni-DATA version 7 is most favorable. Although the low temperature γ' equilibrium fraction are similar between several databases, the predicted γ' fraction at 2000 °F can vary by 7 percent (see Figure 8), though the predicted γ' compositions do not show large departure between databases (see Table 6).

TABLE 5.—ME3 2000 °F MATRIX COMPOSITION COMPARISONS (INCLUDING THE FINE γ' FORMED DURING QUENCH) BETWEEN LEAP AND DATABASE PREDICTION

γ matrix	at.%											
	Ni	Al	Cr	Co	Ti	Mo	W	Nb	Ta	C	RMS	
Ni7	46.4%	**6.0%**	18.5%	21.8%	**2.7%**	3.0%	0.7%	0.4%	0.5%	0.01%	**2.18%**	
Ni5	45.7%	5.6%	19.7%	22.1%	2.4%	3.1%	0.7%	0.3%	0.3%	0.01%	2.89%	
PanNickel	44.3%	5.3%	20.3%	23.0%	2.4%	2.9%	0.8%	0.4%	0.5%	**0.05%**	3.61%	
NIST-Ni	44.7%	5.1%	19.9%	23.8%	2.4%	3.2%	0.8%		0.2%		3.81%	
LEAP	44.9%	**6.7%**	17.5%	21.7%	**3.5%**	3.4%	1.0%	0.5%	0.5%	**0.04%**		
2σ	0.04%	0.02%	0.03%	0.03%	0.01%	0.01%	0.01%	0.01%	0.01%	0.002%		phase fraction at 2000 °F
Ni7 γ'	60.2%	12.0%	2.8%	13.0%	8.8%	0.3%	0.3%	1.3%	1.2%	0.0%		24.8±1.5%
Ni7 MC	0.0%	0.0%	0.2%	0.0%	24.5%	0.2%	0.2%	10.5%	14.5%	47.9%		0.33%
System total	49.6%	7.5%	14.5%	19.5%	4.3%	2.3%	0.6%	0.7%	0.7%	0.2%		
	Ni7	NIST	Ni4~6	Pan-Nickel	TCNI1							
γ' phase fraction	25.5%	29.4%	30.7%	32.3%	8.2%							

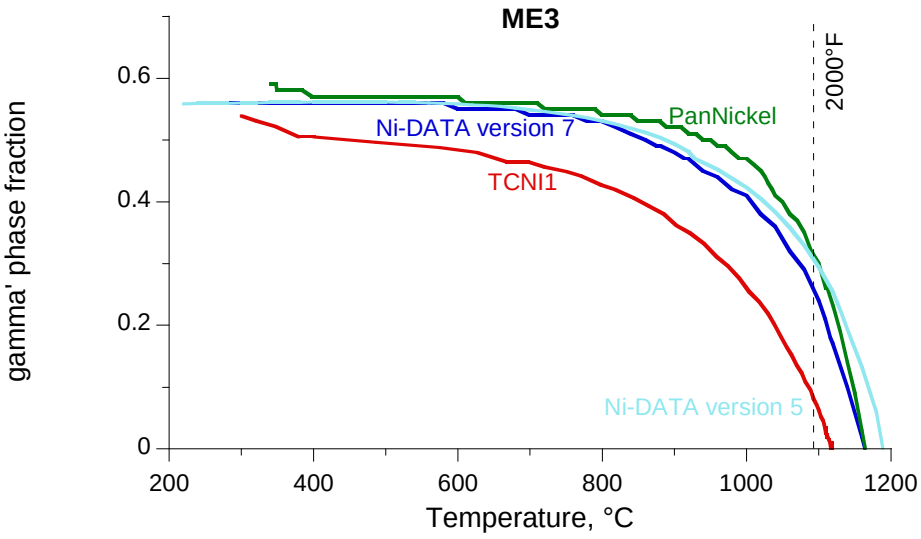

Figure 8.—Calculated equilibrium γ' phase fraction versus temperature with different databases for ME3, showing large variation in 2000 °F prediction.

TABLE 6.—PREDICTED ME3 γ’ COMPOSITIONS AT 2000 °F

Database	ME3 γ’ site-fraction at 2000 °F (1093 °C)
Ni-DATA version 7	$(Ni_{0.80}Co_{0.17}Cr_{0.02})_3$ $(Al_{0.48}Ti_{0.35}Nb_{0.05}Ta_{0.05}Cr_{0.04}Ni_{0.02})$
Ni-DATA version 4~6	$(Ni_{0.79}Co_{0.18}Cr_{0.02})_3$ $(Al_{0.47}Ti_{0.34}Ta_{0.06}Nb_{0.06}Cr_{0.04}Ni_{0.02})$
PanNickel	$(Ni_{0.82}Co_{0.17})_3$ $(Al_{0.49}Ti_{0.33}Cr_{0.06}Nb_{0.05}Ta_{0.04}Ni_{0.01}Mo_{0.01})$
Ni-NIST	$(Ni_{0.86}Co_{0.12}Cr_{0.01})_3$ $(Al_{0.52}Ti_{0.36}Ta_{0.08}Cr_{0.02}Ni_{0.02})$

Using the total sample composition as representing the γ composition at 2000 °F (1093 °C), the root mean square (RMS) between the calculated matrix composition vectors and the solute contents of the LEAP composition vector indicates that Ni-DATA version 7 gives the best agreement (see Table 5). The discrepancy is mainly caused by Al and Ti, which are both underestimated in the calculations. It is noteworthy that the C composition prediction of PanNickel is closest to the measurement, which would result in a higher-fidelity description of the MC precipitation.

The systematic underestimation of Ti in the calculated γ matrix is also noted in QuesTek’s earlier simulations in DARPA-AIM initiative on commercial Ni-base superalloys, as shown in Table 7, and may have to be addressed in this program.

TABLE 7.—COMPOSITION COMPARISONS FOR IN100 AND RENE88DT STUDIED UNDER AIM PROGRAM

		at.%											
IN100 (3step)		Ni	Al	Cr	Co	Ti	Mo	W	Nb	V	Zr	B	C
γ Matrix	PpC	37.5	2.7	28.4	26.1	**0.1**	3.8			1.3	-----	-----	-----
	3DAP	32.0	2.1	30.5	30.8	**0.2**	3.4			0.9	0.007	0.059	0.011
Primary γ'	PpC	61.1	14.1	3.1	12.1	8.8	0.4			0.3	-----	-----	-----
	EDS	63.1	12.4	3.7	11.1	8.0	0.8			0.7			
Secondary γ'	PpC	63.2	15.3	2.7	10.7	7.1	0.5			0.6	-----	-----	-----
	3DAP	62.8	14.7	2.8	10.1	7.9	0.9			0.7	0.003	0.087	0.012
Tertiary γ'	PpC	64.6	17.2	3.0	9.3	3.7	1.1			1.1	-----	-----	-----
	3DAP	63.1	16.3	2.5	9.1	5.3	1.9			1.7	0.052	0.054	0.000
System total		45.7	10.0	13.0	17.0	4.6	1.9			0.8			
Rene88DT (continuous cooling)													
γ Matrix	PpC	50.1	1.4	26.5	16.3	**0.3**	3.6	1.6	0.02			-----	-----
	3DAP	48.0	1.3	28.0	17.0	**0.7**	3.4	1.5	0.01			0.078	0.046
Secondary γ'	PpC	68.0	10.4	2.0	6.5	11.2	0.2	0.6	1.19			-----	-----
	3DAP	71.4	10.3	1.6	4.2	11.2	0.5	0.7	0.01			0.049	0.004
Tertiary γ'	PpC	68.9	11.2	1.8	5.8	10.4	0.2	0.7	1.03			-----	-----
	3DAP	69.4	10.9	2.9	5.1	9.3	1.0	1.3	0.01			0.064	0.026
System total		51.6	2.2	24.6	15.5	1.1	3.4	1.6	0.10				

To prepare the experimental results for PrecipiCalc calibration, the evolution of mean precipitate radius was assessed in Alloy 10, LSHR, and ME3. Eugine Kang, a student at the Northwestern University, conducted image analysis at GRC to measure the γ’ equivalent-circle diameter from SEM images, and the results are summarized in Figure 9. The image analysis indicated a twofold increase of equivalent-circle diameter from intragranular to grain-boundary. In addition, the estimated ME3 γ’ size after solution treat and water quench is about 20 nm in diameter, which is in good agreement with LEAP results of 15 to 30 nm discussed earlier.

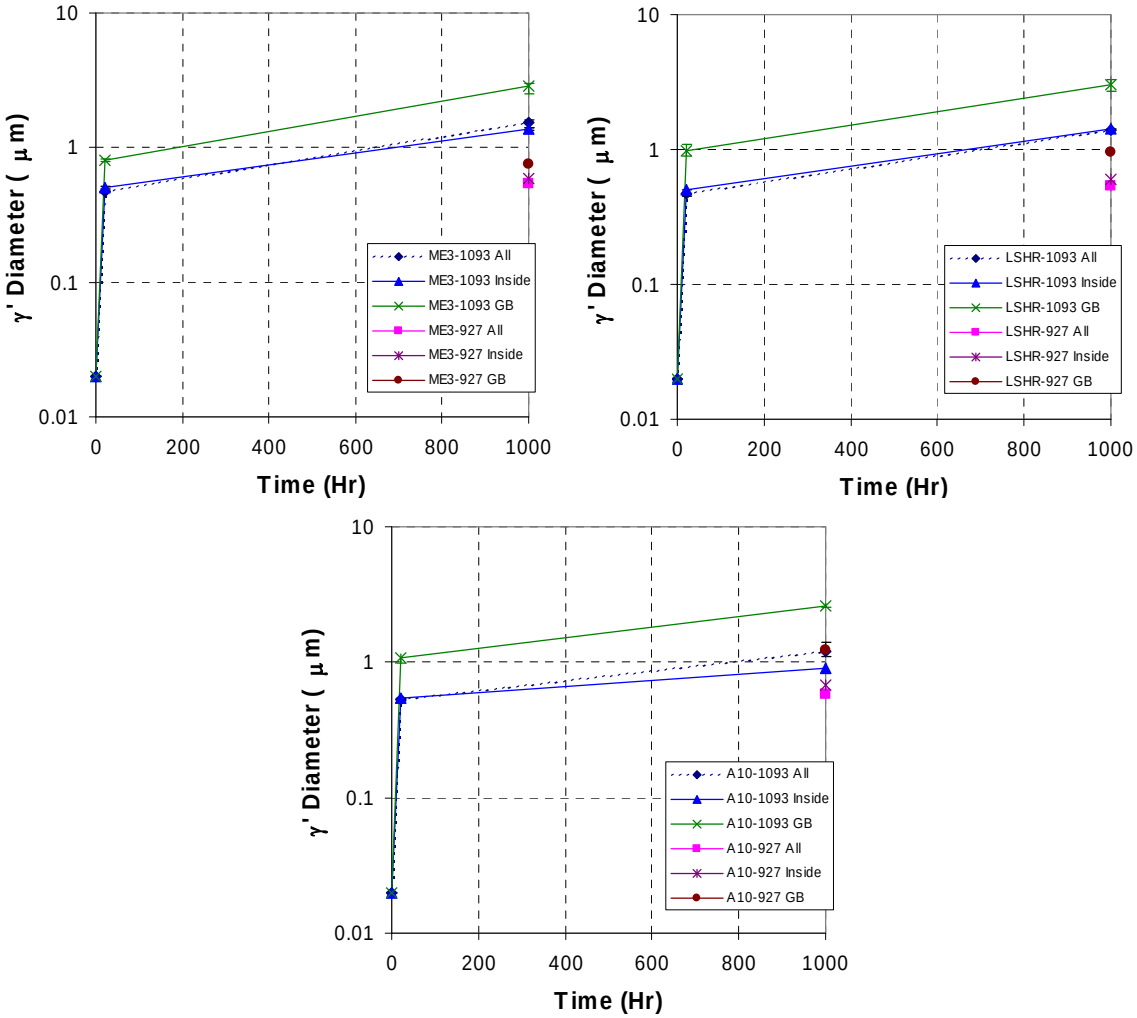

Figure 9.—Summary of isothermal hold experimental results for ME3, LSHR and Alloy10.

Single Sensor DTA Results

For an effective experimental calibration of nucleation related material parameters, Dr. Alexandrov at the Ohio State University conducted Single Sensor Differential Thermal Analysis (SSDTA) measurements to detect the transformation onset temperatures in rapidly cooled arc-melted samples of ME3, LSHR, Alloy10, and RR1000. 40 samples of 1/8-in. diameter pins were analyzed. QuesTek processed the thermograms to reliably derive the γ' precipitation onset.

The first set of SSDTA samples was complicated by the possible solidification segregation as samples were melted and solidified in the arc-melter. Therefore, we alternatively tested the second set using SSDTA in a furnace with Ar or He cooling to avoid melting. The results were still in good agreement with the button-melting experiments. The γ' precipitation onset was measured at 2053 °F (1123 °C) for the first population and at 1567 °F (853 °C) for the second population. The interfacial energy of intragranular γ' precipitates is being calibrated to these SSDTA furnace experiments. The results analyzed by the DTA analysis software are summarized in Table 8. A typical SSDTA curve is presented in Figure 10 showing the first (A) nucleation burst. The transformation onset temperature is the "A_s" column, which will be used to calibrate γ'/γ surface energy in next section, while other identified temperatures are not currently used.

TABLE 8.—RESULTS SUMMARY OF OSU'S SSDTA FURNACE COOL SAMPLES
[Temperatures are in °C.]

Sample	Cooling media	CR1160/1125 C/s	A_S	A_F	Additional effect	A_{F1}	B_S	B_F
A10-2	Ar 11 cf/h	35	1145	1130	----------	989	854	750
A10-3	He 50 cf/h	59	1147	1127	1105-1069			
A10-4	He 50 cf/h	63	1145	1127	1121-1106	964	852	712
LSHR 1	Ar 11 cf/h	49	1123	1103	----------	961		
LSHR 2	Ar 11 cf/h	39	1123	1103	----------	950	853	758
LSHR 3	He 50 cf/h	68	1126	1110	1091-1083	950		
LSHR 4	He 50 cf/h	74	1126	1103	–1091	946	880	751
ME3-1	Ar 11 cf/h	41	1128	1108	----------	893	618	
ME3-2	Ar 11 cf/h	48	1125	1104	----------	899	617	
ME3-3	He 50 cf/h	69	1126	1110	1080-1050	865	587	
ME3-4	He 50 cf/h	70	1126	1103	1087-1027			
RR1000-1	Ar 11 cf/h	28	1108	1090	1007-	901	805	
RR1000-2	Ar 11 cf/h	35	1108	1095	1013-	928	815	
RR1000-3	He 50 cf/h	67	1110	1085	----------	914	862	
RR1000-4	He 50 cf/h	64	1106	1087	1006-	961	884	

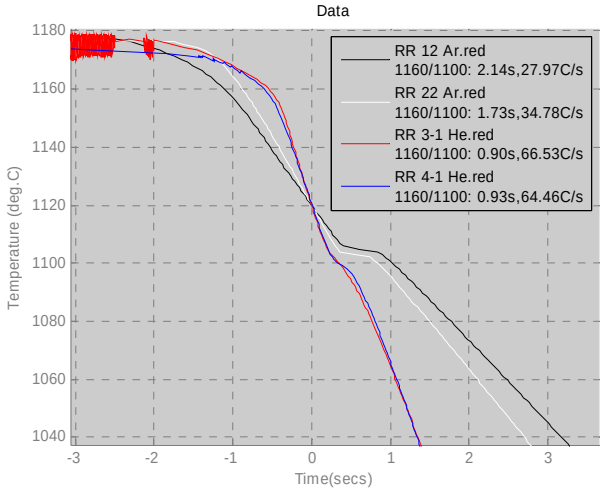

Figure 10.—Typical SSDTA curve for RR1000 showing primary burst event.

Using LEAP, we also analyzed ME3 Ar gas-quenched from 2150 °F (1175 °C). This specimen came from the Single Sensor Differential Thermal Analysis (SSDTA) conducted at Ohio State University, which rapidly acquires the cooling profile. In total, 32 million atoms were analyzed. The overall bulk composition is very close to the expected composition. Larger γ' precipitates, about 40 to 60 nm in diameter, were observed together with smaller gamma' precipitates, about 5 nm or less in diameter. Both sets of precipitates are enhanced predominantly in Ni-Ti-Al, and depleted in Cr-Co. The smaller precipitates showed a flat W composition profile, while the larger precipitates showed a distinct W depletion. A high-resolution SEM analysis on ME3 showed consistent results with the LEAP analysis, see, Figure 11.

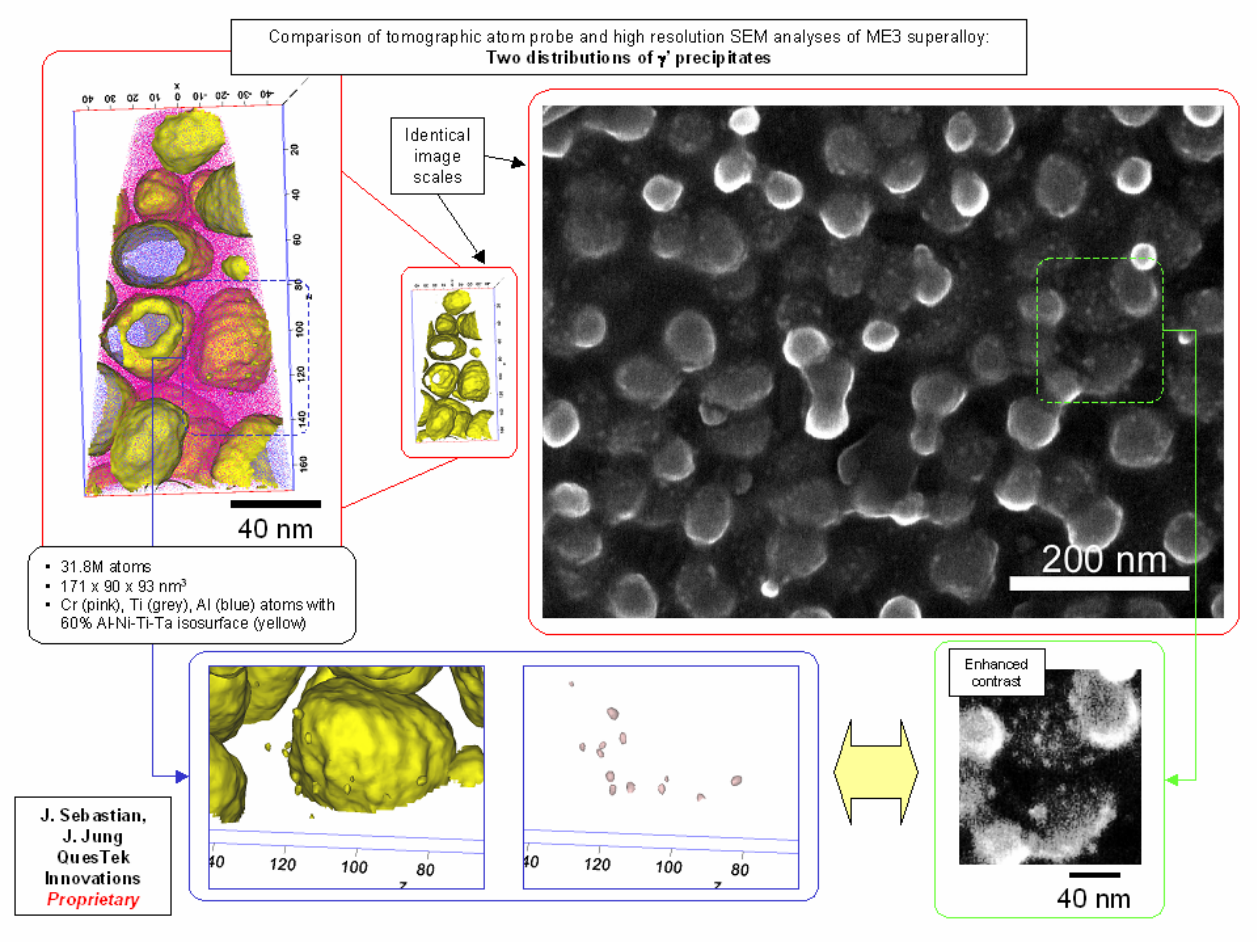

Figure 11.—Result summary of LEAP and high resolution SEM experiments of ME3-1Ar SSDTA sample.

Task 3—γ' Precipitation Modeling

Determination of Modeling Approaches

The data developed in Task 2 are used in γ' precipitation modeling discussed in this section. A logical procedure of calibrating *PrecipiCalc* model parameters is summarized in the following table. Once the fundamental CALPHAD thermodynamics and mobility databases are calibrated through equilibrium age and diffusion couple experiment, SSDTA results of precipitation onset temperatures are used to determine the coherent surface energy (σ_{coh}) and coherent elastic energy (G_{el}), which will be verified with non-isothermal quench results. Then the results of intragrain γ' from equilibrium age experiments will be used to calibrate incoherent surface energy (σ_{incoh}) and interfacial dissipation parameters, while the results of grain boundary γ' will be used to calibrate diffusivity scaling factor ($D_{scale/incoh}$). The coherent to incoherent transition will be justified with available literature models.

Experiments	CALPHAD Thermodynamics and Mobility	Precipitation Kinetics Model Parameters
Equilibrium Age + LEAP and EDS	Matrix/Precipitation Compositions and Phase Fractions	
Diffusion Couple + Microanalysis	$D_{scale/coh}$	
SSDTA		σ_{coh}
		G_{el}
Nonisothermal Quench + LEAP		Check σ_{coh} and G_{el}
Equilibrium Age + SEM/TEM for γ' size and fraction		$\sigma_{incoh,,}$ $D_{scale/incoh}$
		Interfacial Dissipation
Literature		$R_{coh \rightarrow incoh}$

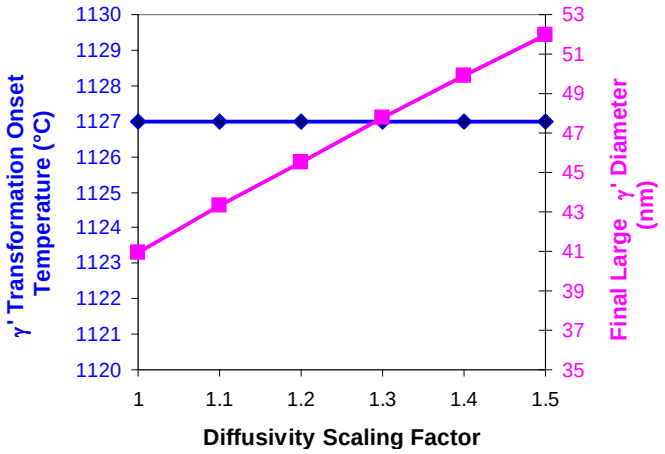

Figure 12.—Impact of diffusivity scaling factor to ME3-1Ar SSDTA PrecipiCalc simulation.

Calibration of PrecipiCalc With SSDTA Results

SSDTA determines the onset of transformation, which is dominated by the nucleation. According to the nucleation theory, the most important material parameters affecting the nucleation rate are driving force (which is determined by the bulk thermodynamics), surface energy and elastic coherency energy—i.e., parameters affecting nucleation energy barrier. In this section, we present the results of calibrating the surface energy, while ignoring the coherency energy.

Unlike the conventional approach using precipitation coarsening results to determine surface energy, the use of onset of transformation has a benefit to remove the dependency of diffusivity. As seen in Figure 12, varying the diffusivity scaling factor in PrecipiCalc does not affect the onset temperature, though it affects the final γ' particle sizes. Hence, our approach of calibrating surface energy with transformation onset temperature removes any uncertainty of diffusivity.

The transformation onset temperatures from the SSDTA experiments were determined from a SSDTA data processing software. It takes the measured temperature versus time, fits the baseline prior to the transformation with a choice of function suitable for describing cooling, and then determines the

departure point of measured data from fitted function. To determine the onset temperature from *PrecipiCalc* simulation with physically equivalent interpretation as closely as possible to SSDTA, here are the steps (see Figure 13 as an example with ME3-1Ar)

(1) Process SSDTA measured temperature profiles to remove the latent heat contribution;

(2) Calculate material compositions relevant to the γ' precipitation from matrix γ phase—the high temperature phases (borides, carbides and undissolved γ') are removed with equilibrium calculations at highest SSDTA measured temperatures using Ni-DATA 7 databases. The undissolved γ' only occurs to Alloy10 samples, and more discussion on this will follow.

(3) Perform *PrecipiCalc* simulations with above information using Ni-DATA 7 and NIST mobility databases, with estimated surface energy;

(4) Collect time (or temperature) evolution results of γ' volume fraction (see Figure 13(a)), and compositions of matrix and γ', compute the time (or temperature) evolution of molar enthalpy (see Figure 13(b));

(5) Compute temperature derivatives of the molar enthalpy with respect to temperature, dH/dT, (see Figure 13(c)),

(6) Determine the transformation onset temperature where dH/dT changes by more than 10 percent of average dH/dT values, with decreasing temperature.

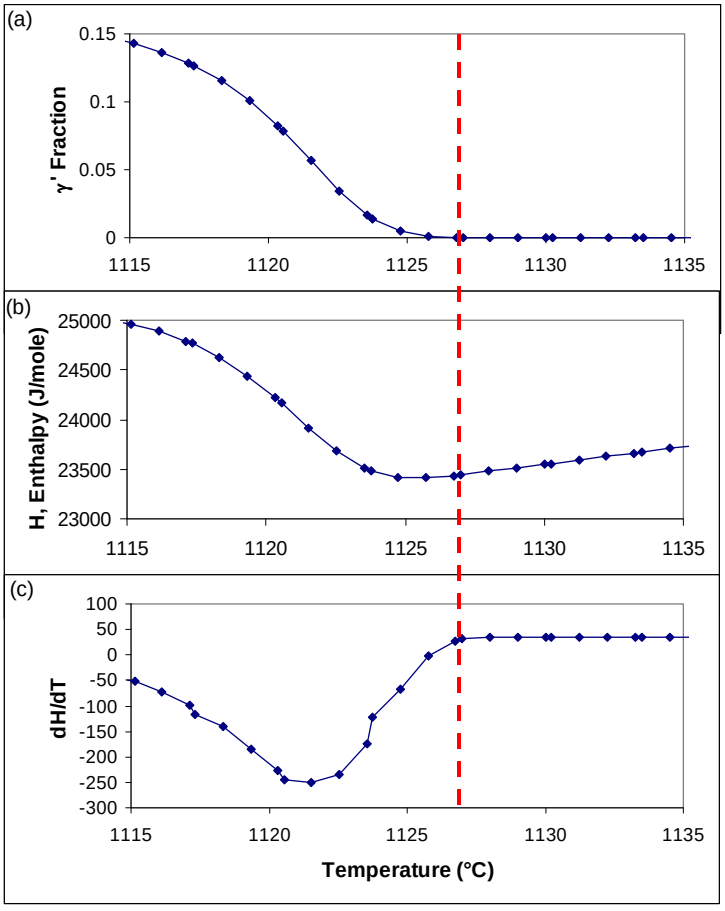

Figure 13.—Determination of transformation onset temperature (vertical red line) from PrecipiCalc simulation with ME3-1Ar using 0.0275 J/m^2 as an example.

Table 9 summarizes the *PrecipiCalc* results and comparison to the SSDTA measured transformation onset temperatures (2nd column), for all 4 alloy samples. We varied the surface energy from 0.0325 to 0.0225 J/m^2 with 0.0025 J/m^2 decrement. The root mean square (RMS) of the difference between prediction and measurement is calculated for each material and estimated surface energy.

TABLE 9.—CALIBRATION OF γ'/γ SURFACE ENERGY WITH THE TRANSFORMATION ONSET TEMPERATURE DETERMINED BY SSDTA

	SSDTA Onset T (°C)	*PrecipiCalc* Simulation, Estimated Surface Energy (J/m^2)									
		0.0325		0.03		0.0275		0.025		0.0225	
		Onset T(°C)	ΔT(°C)	Onset T(°C)	ΔT(°C)	Onset T(°C)	ΔT(°C)	Onset T(°C)	ΔT(°C)	Onset T(°C)	ΔT(°C)
ME3-1Ar	1128			1122.5	5.5	1127	1	1131.2	-3.2		
ME3-2Ar	1125			1123.8	1.2	1126.8	-1.8	1130.9	-5.9		
ME3-3He	1126			1121	5	1125.4	0.6	1130	-4		
ME3-4He	1126			1119.6	6.4	1123.8	2.2	1127	-1		
RMS					4.94		1.54		3.94		
RR1000-1Ar	1108			1096.6	11.4	1100.8	7.2	1105	3	1109.2	-1.2
RR1000-2Ar	1108			1096.9	11.1	1100.7	7.3	1104.5	3.5	1108.2	-0.2
RR1000-3He	1110			1094.5	15.5	1098.7	11.3	1103	7	1107.3	2.7
RR1000-4He	1106			1094.4	11.6	1098.6	7.4	1103.4	2.6	1106.7	-0.7
RMS					12.53		8.48		4.39		1.52
LSHR-1Ar	1123	1123.3	-0.3	1128.6	-5.6	1132.9	-9.9	1137.2	-14.2		
LSHR-2Ar	1123	1123.6	-0.6	1128.9	-5.9	1133.6	-10.6	1137.9	-14.9		
LSHR-3He	1126	1122.1	3.9	1127	-1	1131.9	-5.9	1135.9	-9.9		
LSHR-4He	1126	1121.3	4.7	1126.3	-0.3	1131.3	-5.3	1135.4	-9.4		
RMS			3.07		4.10		8.27		12.35		
A10-2Ar	1145			1136	9.05	1140.8	4.2	1144.7	0.3		
A10-3He	1147			1139.1	7.9	1144.8	2.2	1149.1	-2.1		
A10-4He	1145			1134.9	10.1	1140	5	1144.1	0.9		
RMS					9.06		3.98		1.33		

Based on this analysis, the optimal surface energies (shown with green background) can be determined with minimum RMS for each alloys. That is, 0.0275 J/m^2 for ME3, 0.0225 J/m^2 for RR1000, 0.031 J/m^2 for LSHR (average of 0.0325 and 0.03), and 0.025 J/m^2 for Alloy 10. Note that minimum RMS for LSHR is higher than other alloys, because the experimental transformation onset temperatures for Ar and He cooling are in the opposite trend with conventional wisdom. Furthermore, it is observed that every decrement of 0.0025 J/m^2 in surface energy introduces an increase of about 4 ~5 °C in RMS, which is about the accuracy of SSDTA thermocouple reported by OSU. Hence, the determined surface energy could have a ±0.0025 J/m^2 uncertainty, and then the surface energies of these four alloys are not that different from each other. However, the higher estimated surface energy of Alloy10 could be due to the coherency elastic energy effect, which will be investigated in the 2nd year of this program.

The concern on Alloy10 SSDTA samples was that the unsolutionized large γ' could affect the subsequent nucleation of finer γ'. The amount of undissolved γ' in Alloy10-2Ar SSDTA sample was estimated to be 9.5 percent fraction (see Figure 14), which is comparable to the predicted 8.4 percent equilibrium γ' fraction based on Ni7 database. The calculated onset temperatures of Alloy10 presented in Table 9 were based on the assumption that undissolved γ' does not grow and does not affect the subsequent γ' formation, allowing us to remove the large γ' completely in those *PrecipiCalc* simulations. To confirm our assumption, we performed a Alloy10-2Ar simulation with the presence of large undissolved γ' (with a mean size of about 3 μm and phase fraction of 8.4 percent). Following the quench in SSDTA, the large γ' grows slightly and reduces the available supersaturation. The transformation onset temperature was lower than without the large γ', but only by 1.6 °C (see Figure 15 showing the volume fraction evolution of the fine γ'). Hence, we concluded the assumption to ignore large undissolved γ' is reasonable.

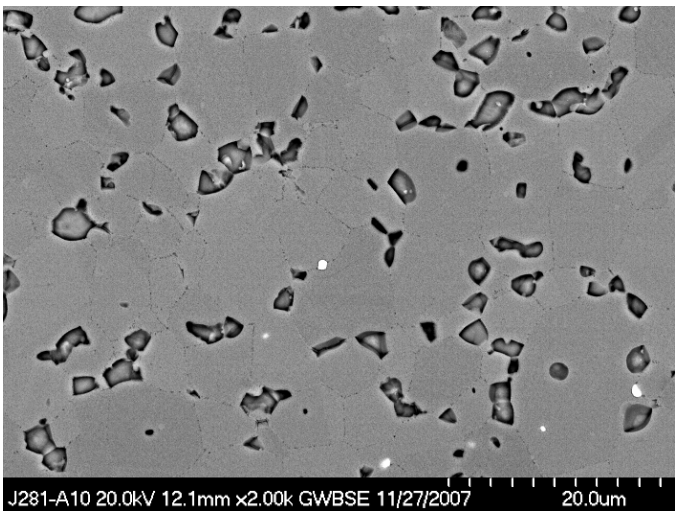

Figure 14.—NASA SEM observation of Alloy10-2Ar SSDTA sample. γ' volume fraction was estimated to be around 9.5 percent.

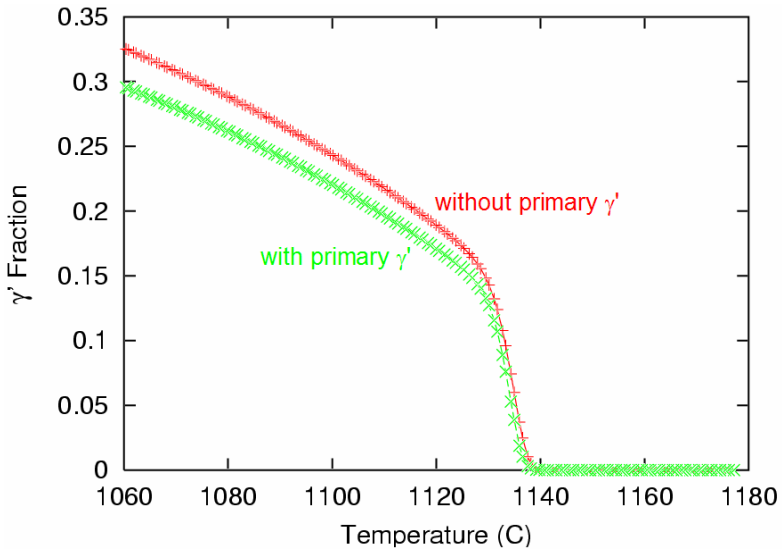

Figure 15.—Comparison of the fine γ' fraction from two PrecipiCalc Alloy10-2Ar simulations with and without primary γ', showing the impact to transformation onset temperature is minimum.

Calibration of PrecipiCalc With Isothermal Hold Experiments

The microstructure of disc alloys aged at 2000 °F (1093 °C) for 1000 hr demonstrated the importance of treating both intragranular and grain boundary precipitation. PrecipiCalc contains both homogeneous and heterogeneous (dislocation and grain boundary) nucleation models. The simulations are being refined for separate nucleation and interfacial mobility parameters for grain boundary behavior in parallel with intragranular precipitation. Parameters specific to heterogeneous nucleation on grain boundary are grain diameter, wetting angle of precipitate interface on grain boundary, and external scaling factor to the nucleation rate to account for uncertainty.

The work in this area is still in progress and will be reported in next report.

Preliminary Conclusions and Next Steps

Results so far indicate the ThermoTech Ni-DATA version 7 thermodynamic database gives the best agreement with measured phase compositions in equilibrated microstructures, providing acceptable accuracy of predicted parameters such as APB energy and interphase misfit. More accurate predictions will likely require incorporation of coherency elastic energy for the high misfit third-generation disc alloys. The fact that the discrepancy of observed critical nucleus composition for the Ni-Al-Cr alloy is in the direction of lower misfit suggests the addition of elastic energy may improve prediction of γ' composition at the nanoscale.

The technical project milestone in Task 1 of the first project year shown in Figure 1 has been achieved. The software development milestone in Task 5 (Figure 1) has also been achieved through the demonstration of suitable *PrecipiCalc* simulation for available data.

Further *PrecipiCalc* simulations will employ separate nucleation and interfacial mobility parameters for grain boundary behavior in parallel with intragranular precipitation.

Future validation studies will include carbide evolution and long-term stability with respect to undesirable TCP phases.

Dr. Olson from QuesTek is planning to attend Superalloys 2008 and prepared an extended abstract titled "Precipitation Model Validation in 3rd Generation Aeroturbine Disc Alloys."

References

1. Database provided by Dr. Ursula Kattner at NIST.
2. Campbell, C.E., W.J. Boettinger, and U.R. Kattner, 2002. *Acta Materialia* 50: 775–792.
3. TCNI1—TCS Ni-based Superalloys database, http://www.thermocalc.com/Products/Databases/TCNI1.htm.
4. Karunaratne, M.S.A. and R.C. Reed, 2003. Interdifusion of the platinum-group metals in nickel at elevated temperature. *Acta Materialia*, 51:2905–2919.
5. Jou, H.-J., P. Voorheese and G.B. Olson, 2004. Computer simulations for the prediction of microstructure/property variation in aeroturbine disks, *Superalloys 2004*, p. 877.
6. Sudbrack, C.K., D. Isheim, R.D. Noebe, N.S. Jacobson, and D.N. Seidman. 2004. The Influence of Tungsten on the Chemical Composition of a Temporally Evolving Nanostructure of a Model Ni-Al-Cr Superalloy. *Microsc. Microanal*. 10: 355–365.
7. Sudbrack, C.K., R.D. Noebe, and D.N. Seidman. 2007. Compositional pathways and capillary effects during isothermal precipitation in a nondilute Ni-Al-Cr alloy. *Acta Materialia*. 55: 119–130.
8. Yoon, K.E., R.D. Noebe, and D.N. Seidman. 2007. Effects of rhenium addition on the temporal evolution of the nanostructure and chemistry of a model Ni–Cr–Al superalloy. II: Analysis of the coarsening behavior. *Acta Materialia*. 55: 1145–1157.
9. DICTRA, Diffusion Controlled TRAnsformation simulation tool http://www.thermocalc.com/Products/Dictra.html
10. TCS Ni-alloys mobility database http://www.thermocalc.com/Products/Databases/Descriptions/DBD_MOBNi1.pdf.
11. http://www.computherm.com/databases.html, PanNickel database from CompuTherm LLC, Madison, WI.
12. Saunders, N. in "Superalloys 1996" eds. R. Kissinger et al. TMS, Warrendale PA, 1996, p. 115. (http://www.thermotech.co.uk/databases.html#Ni-DATA)
13. Thermo-Calc software tool, http://www.thermocalc.com/Products/TCC.html.

REPORT DOCUMENTATION PAGE		Form Approved OMB No. 0704-0188

1. REPORT DATE *(DD-MM-YYYY)*	2. REPORT TYPE	3. DATES COVERED *(From - To)*
01-04-2008	Final Contractor Report	

4. TITLE AND SUBTITLE	5a. CONTRACT NUMBER
Microstructure Modeling of 3rd Generation Disk Alloys	NNC07CB01C
	5b. GRANT NUMBER
	5c. PROGRAM ELEMENT NUMBER

6. AUTHOR(S)	5d. PROJECT NUMBER
Jou, Herng-Jeng	5e. TASK NUMBER
	5f. WORK UNIT NUMBER WBS 698259.02.07.03.03.02

7. PERFORMING ORGANIZATION NAME(S) AND ADDRESS(ES)	8. PERFORMING ORGANIZATION REPORT NUMBER
QuesTek Innovations LLC 1820 Ridge Avenue Evanston, Illinois 60201	E-16471

9. SPONSORING/MONITORING AGENCY NAME(S) AND ADDRESS(ES)	10. SPONSORING/MONITORS ACRONYM(S)
National Aeronautics and Space Administration Washington, DC 20546-0001	NASA
	11. SPONSORING/MONITORING REPORT NUMBER NASA/CR-2008-215199

12. DISTRIBUTION/AVAILABILITY STATEMENT
Unclassified-Unlimited
Subject Category: 26
Available electronically at http://gltrs.grc.nasa.gov
This publication is available from the NASA Center for AeroSpace Information, 301-621-0390

13. SUPPLEMENTARY NOTES

14. ABSTRACT
The objective of this initiative, funded by NASA's Aviation Safety Program, is to model, validate, and predict, with high fidelity, the microstructural evolution of third-generation high-refractory Ni-based disc superalloys during heat treating and service conditions. This initiative is a natural extension of the DARPA-AIM (Accelerated Insertion of Materials) initiative with GE/Pratt-Whitney and with other process simulation tools. Strong collaboration with the NASA Glenn Research Center (GRC) is a key component of this initiative and the focus of this program is on industrially relevant disk alloys and heat treatment processes identified by GRC. Employing QuesTek's Computational Materials Dynamics technology and PrecipiCalc precipitation simulator, physics-based models are being used to achieve high predictive accuracy and precision. Combining these models with experimental data and probabilistic analysis, "virtual alloy design" can be performed. The predicted microstructures can be optimized to promote desirable features and concurrently eliminate nondesirable phases that can limit the reliability and durability of the alloys. The well-calibrated and well-integrated software tools that are being applied under the proposed program will help gas turbine disk alloy manufacturers, processing facilities, and NASA, to efficiently and effectively improve the performance of current and future disk materials.

15. SUBJECT TERMS
Supperalloys disks; Microstructural modeling

16. SECURITY CLASSIFICATION OF:			17. LIMITATION OF ABSTRACT	18. NUMBER OF PAGES	19a. NAME OF RESPONSIBLE PERSON
a. REPORT	b. ABSTRACT	c. THIS PAGE			STI Help Desk (email:help@sti.nasa.gov)
U	U	U	UU	21	19b. TELEPHONE NUMBER *(include area code)* 301-621-0390